Article

Transparent Luminescent Solar Concentrators Using Ln^{3+}-Based Ionosilicas Towards Photovoltaic Windows

Ana R. Frias [1,2], Marita A. Cardoso [1,3], Ana R. N. Bastos [1], Sandra F. H. Correia [1], Paulo S. André [4], Luís D. Carlos [1], Veronica de Zea Bermudez [3] and Rute A. S. Ferreira [1,*]

[1] Department of Physics and CICECO—Aveiro Institute of Materials, University of Aveiro, 3810-193 Aveiro, Portugal; ritafrias@ua.pt (A.R.F.); marita.cardoso@ua.pt (M.A.C.); rita.bastos@ua.pt (A.R.N.B.); sandracorreia@ua.pt (S.F.H.C.); lcarlos@ua.pt (L.D.C.)

[2] Instituto de Telecomunicações, University of Aveiro, 3810-193 Aveiro, Portugal

[3] Department of Chemistry and CQ-VR, University of Traś-os-Montes e Alto Douro, 5000-801 Vila Real, Portugal; vbermude@utad.pt

[4] Department of Electric and Computer Engineering and Instituto de Telecomunicações, Instituto Superior Técnico, Universidade de Lisboa, 1049-001 Lisbon, Portugal; paulo.andre@ist.utl.pt

[*] Correspondence: rferreira@ua.pt; Tel.: +351-234-378-103

check for updates

Abstract: The integration of photovoltaic (PV) elements in urban environments is gaining visibility due to the current interest in developing energetically self-sustainable buildings. Luminescent solar concentrators (LSCs) may be seen as a solution to convert urban elements, such as façades and windows, into energy-generation units for zero-energy buildings. Moreover, LSCs are able to reduce the mismatch between the AM1.5G spectrum and the PV cells absorption. In this work, we report optically active coatings for LSCs based on lanthanide ions (Ln^{3+} = Eu^{3+}, Tb^{3+})-doped surface functionalized ionosilicas (ISs) embedded in poly(methyl methacrylate) (PMMA). These new visible-emitting films exhibit large Stokes-shift, enabling the production of transparent coatings with negligible self-absorption and large molar extinction coefficient and brightness values (~2 × 10^5 and ~10^4 M^{-1}·cm^{-1}, respectively) analogous to that of orange/red-emitting organic dyes. LSCs showed great potential for efficient and environmentally resistant devices, with optical conversion efficiency values of ~0.27% and ~0.34%, respectively.

1. Introduction

The mismatch between AM1.5G spectrum and photovoltaic (PV) cells absorption is one of the critical factors limiting PV performance. To overcome it, several approaches have been proposed. Among them, we highlight luminescent solar concentrators (LSCs) [1–4], a complementary technology to PV cells for use in urban environments [5].

LSCs are devices comprising a transparent matrix in which optically active centers are embedded in. These optically active centers absorb the incident radiation and re-emit it at a specific wavelength. Because of the refractive index contrast between the LSC surface and the air, the emitted radiation is guided in the LSC by total internal reflection to PV cells located at its edges [6,7].

LSCs can be applied over large areas and incorporated into construction elements [8] because LSCs operate similarly under direct and indirect sunlight [9], which is not the case of PV panels that work optimally under direct irradiation. Furthermore, in the built environment, sunlight is diffuse and non-uniform, as it is scattered and reflected by buildings, trees, and clouds reducing the performance of

PV cells [10]. The spectral distribution of diffuse solar radiation has more low wavelength components (particularly in the UV spectral region) than the direct one, which can be better harvested by LSCs [7,9].

The implementation of LSC panels in a noise barrier configuration such as outdoors alongside a roadway in the Netherlands is an illustrative example of the real-world applicability of these devices [8,11,12]. The LSC operation configuration enables PV devices to be embedded in building façades or windows, allowing them to be transformed into energy-harvesting units, contributing to the development of zero-energy buildings [2]. Furthermore, LSCs will also impact wearable fabrics and mobile energy [13]. In fact, previous studies report the possibility of charging low-voltage devices, such as mobile phones, sensors, and Wi-Fi routers by using LSCs as windows [14].

LSCs appeared in the late 1970s with the goal of overcoming the mismatch between the full solar spectrum on Earth and the semiconductor material used in PV cell manufacture [1]. The first LSCs reported were planar devices [6,15,16] containing optical active centers with absorption complementary to that of the semiconductor material of the PV cells, and emission tuned in the PV cell absorption spectral range.

The performance of LSCs may be determined by the balance between the optical features of the emitting layer (quantified by the optical conversion efficiency, η_{opt}) and the device geometry (quantified by the geometrical gain $G = A_s / A_e$, A_s and A_e being the surface collection and edge areas of the LSC, respectively). In terms of material selection towards η_{opt} optimization, several challenges are still open. Quantum dots (QDs) display tunable absorption and emission spectra with large Stokes-shift and have been widely used in LSCs [17–21], despite concerns about toxicity [22,23]. Ln^{3+}-based complexes display attractive properties for LSCs due to tunable absorption range controlled by an adequate choice of the ligands, and high-emission quantum yield covering the visible/NIR spectral region depending on the selected Ln^{3+} ion. Moreover, compared with organic dyes, the large ligands-induced Stokes-shift is advantageous to prevent self-absorption losses. However, Ln^{3+}-based complexes also show low thermo/photo-stability and poor mechanical properties, which constitute a barrier to its application [24].

This undesirable feature of Ln^{3+}-based complexes can be overcome by introducing ionic liquids (ILs), which are molten salt with melting temperature below 100 °C and several exciting properties, such as high thermal stability, extremely low volatility, high ionic conductivity, wide liquid range and designable solvents [25,26]. Anchorage of the organic ionic group to a silica surface through a covalent bond allows the production of ionosilicas (ISs), an attractive subclass of organosilicas that combine the properties of silica materials and ILs [27]. The resulting organic-inorganic hybrid materials are endowed with improved physical-chemical properties of synergies arising from both components (silica and IL) [28]. A prime advantage of ISs is that their properties may be easily tuned through a fine control of the chemical structure of the IL, i.e., a judicious choice of the IL cation and anion. ISs applications has been highlighted in the fields of separation, catalysis, molecular recognition [27] and have been also proposed as good candidates for organic light emitting diodes and LSCs [28,29].

To enable an easy process and control the morphology of the optically active centers, poly methyl methacrylate (PMMA) was chosen due to attractive features such as low cost, environmentally friendly nature, high optical transparency [29], high resistance to UV radiation exposure and several chemical treatments, exceptional performance in all-weather conditions and extensive use in construction as a lightweight window material and optical fiber [30]. Moreover, PMMA is an easy material to work with in the laboratory, not presenting any noteworthy risk concerns, which allows high doping concentrations before concentration quenching occurs [31] and transforms them into high-optical-quality transparent matrices with no degradation in their photoluminescence efficiency [30]. Even if PMMA exhibits relatively poor mechanical resistance [31], that can be overcome by the ISs silica nature. The combination of ISs and PMMA can result in transparent, flexible, and luminescent materials, presenting fascinating prospects in luminescent photovoltaic applications.

The field of PV devices is in constant development and special focus has been given to c-Si PV cells (the most used technology in the photovoltaic field), and to perovskite-based technologies,

which represent a novel promising approach due to the unprecedented efficiency increase within a short period of time (<10 years) [32]. Nevertheless, both types of PV cells present low efficiency values in the UV spectral range and, in the case of the perovskites-based cells, stability issues upon exposure to air, moisture and UV radiation are a serious drawback [33,34]. Taking into account the aforementioned limitations, coupling these PV cells to LSCs could, thus, be an attractive strategy.

In this work, LSCs based on Ln^{3+} (Eu^{3+} and Tb^{3+})-doped surface functionalized ISs (Figure 1) embedded in PMMA matrices were prepared. Here, sol-gel-derived ISs comprising a pendant imidazolium-terminated alkyl chain and a luminescent Ln^{3+}-based anionic complex as counter-ion were synthesized. The new materials exhibit large Stokes-shift enabling the production of transparent materials with negligible self-absorption allowing efficient solar radiation harvesting and conversion.
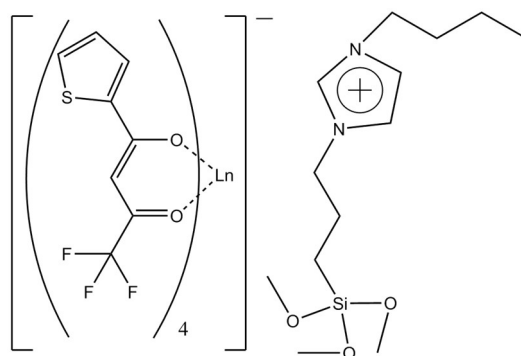
Figure 1. Schematic structure of the non-hydrolyzed lanthanide (Ln = Tb/Eu)-based ISs: 1-butyl-3-[3-(trimethoxysilyl)propyl]imidazolium tetra(2-thenoyltrifluoroacetonate)terbate/europate (III) [B(TMSP)Im][Ln(TTA)$_4$].

2. Materials and Methods

N-butylimidazole (BIm, 98%, Sigma-Aldrich), (3-chloropropyl)trimethoxysilane (CPTMS, 97%, Sigma-Aldrich), terbium(III) chloride hexahydrate (TbCl$_3$·6H$_2$O, 99.9%, Acros Organics), europium(III) chloride hexahydrate (EuCl$_3$·6H$_2$O, 99.99%, Sigma-Aldrich), 2-thenoyltrifluoroacetone (TTA) (99%, Sigma-Aldrich), methyl methacrylate (MM) (99%, Acros), benzoyl peroxide (97%, Alfa Aesar), anhydrous ethyl acetate (EtOAc, 98.8%, Sigma-Aldrich), ethanol (EtOH) (99.8%, Fisher Chemical) tetrahydrofuran (THF, Sigma-Aldrich), sodium hydroxide (NaOH, Merck), and dichloromethane (DCM, HPLC grade, Fisher Chemical and ≥99.9%, Honeywell Riedel-de Haën) were used as received. High purity distilled water was used in all experiments. The detailed preparation of 1-butyl-3-[3-(trimethoxysilyl)propyl]imidazolium chloride ([B(TMSP)Im]Cl), 1-butyl-3-[3-(trimethoxysilyl)propyl]imidazolium tetra(2-thenoyltrifluoroacetonate)terbate/europate (III) [B(TMSP)Im][Ln(TTA)$_4$] compounds and of the corresponding ionosilicas (IS-Ln) is detailed in Supplementary Information [35]. To enable films processing, the IS-Ln were incorporated into PMMA solutions with a concentration of $X = 20\%$ wt. ($X = m_{IS-Ln}/m_{PMMA}$). These samples will be hereafter designated as PMMA-Ln (Ln = Tb, Eu for Tb^{3+} and Eu^{3+}-based materials, respectively). These PMMA-Ln materials were deposited on the glass substrates (7.5 × 2.0 × 0.1 cm^3) by drop-casting using 0.66 mL of the solution. Then, the films were left to dry in an atmosphere rich in DCM (to ensure a slow drying of the material and, thus, yield a transparent film) at room temperature for 5 h. The thickness values of the active layers of the LSCs produced, measured by spectroscopic ellipsometry in three distinct regions of the surface, were 10.70 ± 0.05 and 5.10 ± 0.09 μm for PMMA-Tb and PMMA-Eu, respectively (Table S1 in Supplementary Information).

The materials optical characterization was performed through room temperature photoluminescence recorded with a Fluorolog-3, Horiba Scientific equipment. The absolute emission quantum yield values (q) were measured at room temperature using Quantaurus-QY Plus C13534, Hamamatsu system, with an accuracy within 10%. UV/visible absorption spectra

were recorded using a Lambda 950, Perkin-Elmer spectrometer. The molar extinction coefficient was calculated through using the Beer Lambert law ($A = \varepsilon c l$, where A is the absorbance, ε is the molar extinction coefficient in $M^{-1} \cdot cm^{-1}$, c is the concentration of the absorbing species in M and l is the optical path in cm) [36], and the molar brightness ($B(\lambda) = \varepsilon(\lambda)q(\lambda)$, in $M^{-1} \cdot cm^{-1}$) were calculated for the highest absorption wavelength. The spectroscopic ellipsometry measurements were made using an AutoSE ellipsometer (Horiba Scientific) in the wavelength range of 450 to 850 nm. Three measurements were performed in each sample. The used structural model is described in detail in the Supplementary Information. Further details about the optical characterization equipment and techniques can be found in the Supplementary Information. To quantify η_{opt} from experimental data, the following definition was considered [37]:

$$\eta_{opt} = \frac{P_{out}}{P_{in}} = \frac{I_{SC}^L V_0^L}{I_{SC} V_0} \frac{A_e}{A_s} \frac{\eta_{solar}}{\eta_{PV}}, \tag{1}$$

where I_{SC}^L and V_0^L are the short-circuit current and the open-circuit voltage of the PV device when coupled to the LSC (I_{sc} and V_0 are the corresponding values of the PV device exposed directly to the solar radiation), η_{solar} is the efficiency of the PV device relatively to the total solar spectrum and η_{PV} is the efficiency of the PV device at the LSC emission spectral range.

The experimental η_{opt} values were determined by illuminating the top surface of the LSCs with simulated AM1.5G illumination (Model 10500, Abet Technologies). The optical power at the LSC output was estimated using a c-Si PV cell (KXOB22-01X8F, IXYS, presenting a maximum external quantum efficiency (EQE) around 80%, Figure S1 in Supplementary Information) with a mask matching A_e dimensions. The I_{sc} and V_0 values were measured using a source meter device (2400 SourceMeter source measure unit (SMU) Instruments, Keithley). A reflective tape (Figure S2 in Supplementary Information) was used on the free edges and in the rear side of the LSCs. The mismatch between the AM1.5G solar spectrum and that of the solar simulator was taken into consideration [38].

The power conversion efficiency (PCE) was calculated through:

$$PCE = \frac{P_{out}^{el}}{P_{in}} = \frac{I_{SC}^L V_0^L FF}{A_S \int_{\lambda_1}^{\lambda_2} I_{AM1.5G}(\lambda) d\lambda}, \tag{2}$$

where P_{out}^{el} and $FF = 0.75$ are the PV device output electrical power and fill factor, respectively.

3. Results

3.1. Optical Characterization

Figure 2a shows the room temperature emission spectra of the PMMA-Ln samples excited at the wavelength that maximizes the emission intensity. The emission spectra of PMMA-Tb and PMMA-Eu are dominated by the $^5D_4 \rightarrow {}^7F_{6-3}$ and $^5D_0 \rightarrow {}^7F_{0-4}$ transitions, respectively. In terms of energy, relative intensity, full-width-at-half-maximum, and number of Stark components, these spectra resemble those observed for the IS-Ln compounds (Figure S3 in Supplementary Information) pointing out that the IS-Ln compounds preserve their local structure after the PMMA incorporation. Independently of the selected excitation wavelength (270–380 nm), no sign of the PMMA intrinsic emission [39] could be observed, which readily suggests efficient PMMA-to-ligand/Ln^{3+} energy transfer [40].
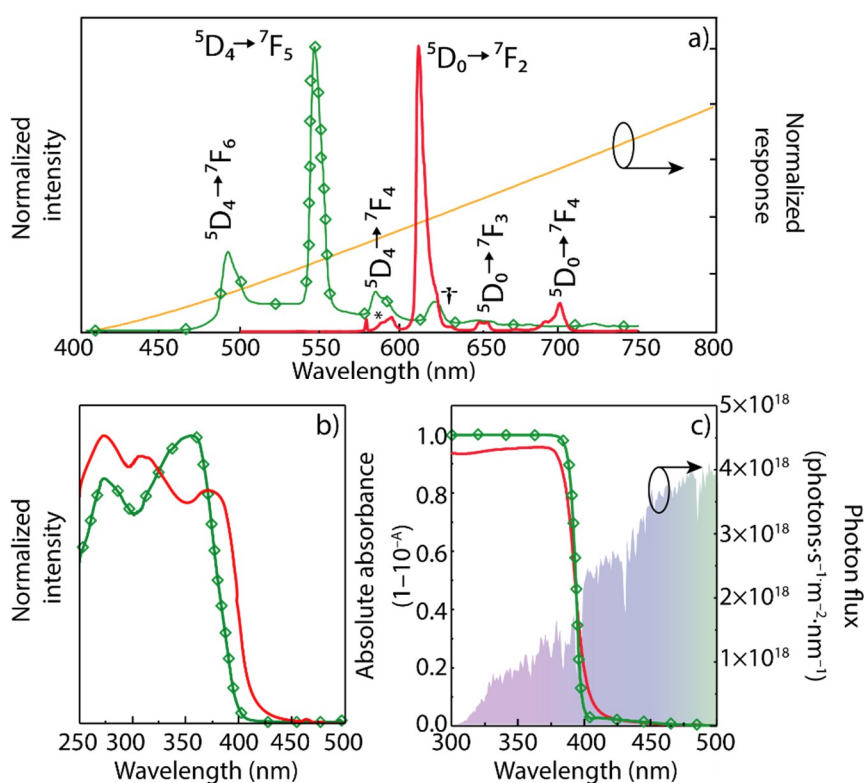
Figure 2. (**a**) Emission spectra excited at 360 nm for PMMA-Tb (green line with diamonds) and 380 nm for PMMA-Eu (red solid line). The asterisk marks the region of the superposition between the Eu^{3+} $^5D_0 \rightarrow {}^7F_{0-1}$ and the Tb^{3+} $^5D_4 \rightarrow {}^7F_4$ transitions. The cross marks the region of the superposition between the Eu^{3+} $^5D_0 \rightarrow {}^7F_2$ and the Tb^{3+} $^5D_4 \rightarrow {}^7F_3$ transitions. The orange line is the normalized c-Si PV devices absorption curve; (**b**) Excitation spectra for PMMA-Tb monitored at 545 nm and PMMA-Eu monitored at 612 nm. (**c**) Absorption spectra for PMMA-Tb, PMMA-Eu, and AM1.5G photon flux (the color code for (**b**) and (**c**) is the same as in (**a**)).

The excitation spectra were monitored around the more intense transitions, namely $^5D_4 \rightarrow {}^7F_5$ (PMMA-Tb) and $^5D_0 \rightarrow {}^7F_2$ (PMMA-Eu), Figure 3b. In the range of interest (300 to 800 nm), the spectra show two main components peaking at 320 and 360/380 nm ascribed to the $\pi - \pi^*$ electronic transition of the TTA ligands [41,42]. Apart from changes in the relative intensity, the UV-visible absorption spectra reveal the same components detected in the excitation spectra, Figure 2c. From the analysis of the emission and excitation spectra, large ligands-induced Stokes-shift of ~10000 cm^{-1} for PMMA-Tb and PMMA-Eu is found, as desirable for LSCs applications.
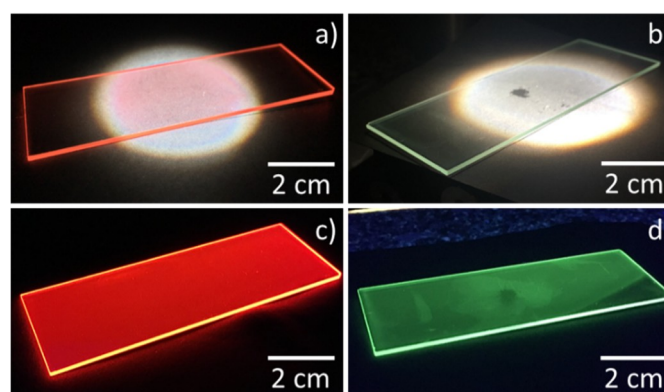
Figure 3. Photographs of the LSCs based on (**a,c**) PMMA-Eu and (**b,d**) PMMA-Tb under AM1.5G (top) and UV radiation at 365 nm (bottom).

The emission decay curves were monitored under UV excitation (380 nm) revealing a single exponential behavior (Figure S4 in Supplementary Information). From the best data fit, the lifetime values were estimated (Table 1).

Table 1. $^5D_4$ (PMMA-Tb) and $^5D_0$ (PMMA-Eu) lifetime values (τ, $\times 10^{-3}$ s), integral overlap (O, $\times 10^{19}$ photons·s^{-1}·m^{-2}), absolute emission quantum yield (q), molar extinction coefficient (ε, $\times 10^5$ M^{-1}·cm^{-1}) and brightness (B, M^{-1}·cm^{-1}) of PMMA-Ln.

Film	τ	O	ε	q	B
PMMA-Tb	0.060 ± 0.001	9.0	2.2	0.016 ± 0.002	3.5×10^3
PMMA-Eu	0.553 ± 0.006	8.7	1.1	0.305 ± 0.030	3.8×10^4

The emission properties of the PMMA-Ln films were further quantified through the measurement of the absolute emission quantum yield (q, Table 1) as a function of the excitation wavelength (270–385 nm for PMMA-Ln). The q values although lower than those previously reported for PMMA doped with Eu(tta)$_3$(phen), with $q = 0.73\pm0.06$ [43], and [Eu(hfac)$_3$(DPEPO)] (hfac=hexafluoroacetylacetonate and DPEPO=bis(2-(diphenylphosphino)phenyl)ether oxide, with values of $q = 0.85\pm0.09$ [44], are of the same order of that of a material consisting of PMMA and the 1-hexyl-3-methylimidazolium bis(trifluoromethylsulfonyl)-imide ionic liquid with Eu(tta)$_3$(phen), which presented $q = 0.46$ [45].

Featuring PV related applications, it is pertinent to quantify the light harvesting ability of the LSCs [37]. In particular, the overlap integral between the materials absorbance and the solar radiation available for PV harvesting is of interest. The overlap integral is given by Equation (3) [46]:

$$O = \int_{\lambda_1}^{\lambda_2} \Phi_{AM1.5G}(\lambda) \times \left(1 - 10^{-A(\lambda)}\right) d\lambda \tag{3}$$

where λ_1 (300 nm) and λ_2 (800 nm) are the limits of the region of spectral overlap between the absorption spectrum of each sample and the AM1.5G spectrum, $\Phi_{AM1.5G}$ is the AM1.5G photon flux and A is the absorbance of the PMMA-Ln samples. The overlap regions between the absorption spectra and the AM1.5G photon flux can be observed in Figure 2c, whose calculated O values (Table 1) indicate that both coatings have the ability to absorb ~2% of the solar photon flux [3] on the surface of the Earth (4.3×10^{21} photons·s^{-1}·m^{-2}). To complement the quantification of the light harvesting ability, the molar extinction coefficient (ε) was estimated, Table 1. The values found for all the films are quite large for Ln^{3+}-based complexes, whose values are of the order of 10^4 M^{-1}·cm^{-1} in the UV spectral region [47–52].

Molar brightness, B, is a measure of the light emission efficiency and light harvesting ability, allowing the comparison of the contribution of both parameters across distinct samples. In the present case, as similar ε values are found for all the films, the larger B value is governed by the larger quantum yield of PMMA-Eu. We note that in this case, B is of the order of 10^4 M^{-1}·cm^{-1} which is similar to those reported for orange/red-emitting organic dyes that are known for their light harvesting ability [53,54]. Taking into account the optical properties, namely the largest integral overlap and brightness values, PMMA-Eu is the coating with higher potential for LSC applications, as detailed below.

3.2. LSCs

The PMMA-based films incorporating Ln^{3+}-based ISs were used to fabricate LSCs. A layer of each material was deposited on the top surface of a glass substrate (Figure 3). The light emitted at the surface of the PMMA-Tb and PMMA-Eu-based LSCs are guided and concentrated towards the substrate edges (Figure 3 and Figure S5 in Supplementary Information). As presented in Figure 3, light emission and guidance to the edges occurs both under AM1.5G and UV radiation. The performance of the LSCs was quantified by the estimation of η_{opt} through Equation (1), yielding values of η_{opt}~0.27% and ~0.34% for the LSCs based on PMMA-Tb and PMMA-Eu, respectively (Table S2 in Supplementary Information).

We note that in some works, the authors used a distinct expression to calculate η_{opt}, considering only the ratio between I_{SC} and I_{SC}^{L}, yielding to overestimated results [19–21]. Nevertheless, to enable a comparison with the literature, we calculate η_{opt} using such expression, yielding η_{opt} values of 0.29% and 0.68% for PMMA-Tb and PMMA-Eu, respectively. In addition, the effective contribution of the LSCs on the generation of electric current was evaluated by calculating the PCE values, through Equation (2), yielding values of 7.8×10^{-4}% and 1.9×10^{-3}% for PMMA-Tb and PMMA-Eu LSCs, respectively.

3.3. Modelling

A Monte Carlo ray-tracing model was used to simulate the performance of the LSCs, in which the photon propagation follows geometrical optical laws [55]. The details of the simulation are described elsewhere [14] and in the Supplementary Information. The input data for Monte Carlo ray-tracing simulation are the solar spectrum AM1.5G (280–1600 nm), the absorption, and emission spectra, the absolute emission quantum yield and dispersion curve of the PMMA-Ln samples (Figure S6 and Figure S7 in Supplementary Information).

The performance of the LSCs was simulated placing the PV cell on one of the edges of the LSC that is composed of a glass substrate with an active layer deposited on top of it. For simulation purposes, the η_{opt} is defined by the energy emitted (per unit of time) from the edge of the LSC divided by the solar energy falling on the LSC (per unit of time), as stated in Equation (1). The simulations were performed for the LSCs with dimensions of $7.50 \times 2.00 \times 10^{-3}$ cm^3 as function of the optically active layer properties. The η_{opt} values were predicted considering all the photons reaching the edge (η_{opt}, %) and considering only the fraction of converted photons (η'_{opt}, %), Table S3 in Supplementary Information. The η_{opt} and η'_{opt} values corroborate the experimental values taking into account the direct radiation that reaches the PV device through the LSC. Nevertheless, the simulated value (0.23% for PMMA-Eu) is close to the experimental one, confirming that this model fits well our experimental conditions.

The real applicability of the proposed LSCs requires the estimative of their performance, at larger collection surface ($7.50 \times 10^{-4} < A_s < 1.05$ m^2), Figure S8 in Supplementary Information. As the collection surface increases, η_{opt} remains approximately constant (0.23±0.01%). The output electrical power of the PV device (P_{out}^{el}) is related to A_s through:

$$P_{out}^{el} = \eta_{Si}\eta_{opt}A_s I_{AM1.5} \tag{4}$$

where η_{Si} = 4% is the Si PV cell efficiency and $I_{AM1.5G}$ = 1000 Wm^{-2}. To attain P_{out}^{el} comparable to the one delivered by an USB port (Table S4 in Supporting Information) an LSC with A_s up to 2.8×10^{-1} m^2 is required, Figure S8 in Supplementary Information.

4. Discussion

Following previous work of the group on Ln^{3+}-based LSCs [4,38,56,57], LSCs made of PMMA doped with Ln^{3+} (Eu^{3+}, Tb^{3+})-based ISs processed by the sol-gel method were here studied. These optically active centers display absorption in the UV component of the solar irradiance on Earth (absorption at 300–400 nm, which allows the fabrication of fully transparent LSCs) and with the emission spectra centered in the visible spectral regions, resonant with c-Si PV devices absorption.

The LSCs showed promising results, towards the use of these novel materials as transparent PV windows for urban integration of light harvesting devices, for future zero-energy buildings. Moreover, the use of PMMA doped with Ln^{3+}-based ISs as optically active centers in LSCs demonstrates the potential of ISs in the direction for highly efficient and environment-resistant devices, with the additional advantage of presenting lower toxicity than the case of QDs technology. Nevertheless, the presented devices need further improvements in order to increase η_{opt} and PCE values, namely excitation deviation towards the blue and quantum yield increase. Future work should

also be focused on the synthesis of efficient NIR-emitting optically active centers, with emission around 1100 nm, matching c-Si bandgap.

Supplementary Materials: The following are available online at http://www.mdpi.com/1996-1073/12/3/451/s1, Figure S1. EQE curve of the c-Si PV cell used in this work, Figure S2. Reflectance curve of the reflective tape used in the LSCs, Figure S3. Room temperature emission spectra PMMA-Eu and IS-Eu excited at 385 and 390 nm, respectively, Figure S4. Room temperature emission decay curves for (a) PMMA-Tb and (b) PMMA-Eu excited at 380 nm and monitored at 544 and 612 nm, respectively. The solid lines represent the best fit to the data ($r^2 > 0.93$) using a single exponential function. The respective residual plots are shown on the right-hand side, Figure S5. Emission of the LSCs collected at the edges of the LSCs based on (a) PMMA-Tb and (b) PMMA-Eu. The emission spectra at the edges of the LSCs spectra were acquired using a spectrometer OceanOptics Maya 2000 Pro coupled with an optical fiber under AM1.5G radiation, Figure S6. Ellipsometric parameters I_s (open circles) and I_c (open triangles) measured for (a) PMMA, (b) PMMA-Tb and (c) PMMA-Eu. The solid lines represent the data best fit, Figure S7. Dispersion curves measured for PMMA, PMMA-Tb, and PMMA-Eu, Figure S8. Monte Carlo ray-tracing optical conversion efficiency as function of the LSC surface area and predicted output electrical power. A constant thickness of 10^{-3} m (typical value for a glass window) was considered in all the simulations. The symbols refer to the A_s value needed to attain P_{out}^{el} comparable to the one delivered by an USB port and needed to charge the low-voltage devices indicated, Materials synthesis and processing details, Modelling details, Table S1. Thickness of the active layer of the LSCs deposited on glass, Table S2. Quantification of parameters expressed in Equation (1) of the manuscript for η_{opt} calculation, Table S3. Simulated optical conversion efficiency values considering all the photons reaching the edge (η_{opt}, %) and only the converted photons (η'_{opt}, %) for the LSCs based on PMMA-Ln, Table S4. Typical values for the electrical power interval available at a USB port and required to charge small electronic devices, Table S5. Ellipsometric parameters from the Cauchy absorbent model, Equation (S1) in the Supplementary Information.

Author Contributions: Conceptualization, P.S.A., L.D.C., V.Z.B. and R.A.S.F.; Funding acquisition, L.D.C. and R.A.S.F.; Investigation, A.R.F., M.A.C., A.R.N.B. and S.F.H.C.; Project administration, L.D.C. and R.A.S.F.; Resources, L.D.C. and R.A.S.F.; Supervision, L.D.C. and R.A.S.F.; Writing—original draft, A.R.F. and M.A.C.; Writing—review and editing, S.F.H.C., P.S.A., L.D.C., V.Z.B. and R.A.S.F.

Conflicts of Interest: The authors declare no conflict of interest.

References

1. Huang, X.; Han, S.; Huang, W.; Liu, X. Enhancing solar cell efficiency: the search for luminescent materials as spectral converters. *Chem. Soc. Rev.* **2013**, *42*, 173–201. [CrossRef] [PubMed]

2. McKenna, B.; Evans, R.C. Towards efficient spectral converters through materials design for luminescent solar devices. *Adv. Mater.* **2017**, *29*, 1606491. [CrossRef] [PubMed]

3. Bünzli, J.-C.G.; Chauvin, A.-S. Lanthanides in Solar Energy Conversion. In *Handbook on the Physics and Chemistry of Rare-Earths*; Bünzli, J.-C.G., Pecharsky, V.K., Eds.; Elsevier B.V.: Amsterdam, The Netherlands, 2014; Volume 44, pp. 169–281.

4. Correia, S.F.; de Zea Bermudez, V.; Ribeiro, S.J.; Andre, P.S.; Ferreira, R.A.; Carlos, L.D. Luminescent solar concentrators: Challenges for lanthanide-based organic-inorganic hybrid materials. *J. Mater. Chem. A* **2014**, *2*, 5580–5596. [CrossRef]

5. Kaniyoor, A.; McKenna, B.; Comby, S.; Evans, R.C. Design and response of high-efficiency, planar, doped luminescent solar concentrators using organic–inorganic di-Ureasil waveguides. *Adv. Opt. Mater.* **2016**, *4*, 444–456. [CrossRef]

6. Weber, W.H.; Lambe, J. Luminescent greenhouse collector for solar-radiation. *Appl. Opt.* **1976**, *15*, 2299–2300. [CrossRef] [PubMed]

7. Reisfeld, R.; Neuman, S. Planar solar energy convertor and concentrator based on uranyl-doped glass. *Nature* **1978**, *274*, 144–145. [CrossRef]

8. Kanellis, M.; de Jong, M.M.; Slooff, L.; Debije, M.G. The solar noise barrier project: 1. Effect of incident light orientation on the performance of a large-scale luminescent solar concentrator noise barrier. *Renew. Energy* **2017**, *103*, 647–652. [CrossRef]

9. Debije, M.G.; Rajkumar, V.A. Direct versus indirect illumination of a prototype luminescent solar concentrator. *Sol. Energy* **2015**, *122*, 334–340. [CrossRef]

10. Li, Y.; Zhang, X.; Zhang, Y.; Dong, R.; Luscombe, C.K. Review on the Role of Polymers in Luminescent Solar Concentrators. *J. Polym. Sci., Part A: Polym. Chem.* **2019**, *57*, 201–215. [CrossRef]

11. Debije, M.G.; Tzikas, C.; Rajkumar, V.A.; de Jong, M.M. The solar noise barrier project: 2. The effect of street art on performance of a large scale luminescent solar concentrator prototype. *Renew. Energy* **2017**, *113*, 1288–1292. [CrossRef]

12. Debije, M.G.; Tzikas, C.; de Jong, M.M.; Kanellis, M.; Slooff, L.H. The solar noise barrier project: 3. The effects of seasonal spectral variation, cloud cover and heat distribution on the performance of full-scale luminescent solar concentrator panels. *Renew. Energy* **2018**, *116*, 335–343. [CrossRef]

13. Lim, I.-G.; Kang, S.-W.; Hyoung, C.; Park, K.-H.; Kim, S.-E.; Kang, T.-Y.T.-W.; Park, H.-I.; Hwang, J.-H.; Choi, B.-G.; Kang, T.-Y.T.-W.; et al. Wearable Wireless Power Transmission Apparatus and Wireless Power Transmission Method Using the Same. U.S. Patent US20140015470A1, 16 January 2014.

14. Frias, A.R.; Pecoraro, E.; Correia, S.F.H.; Minas, L.M.G.; Bastos, A.R.; García-Revilla, S.; Balda, R.; Ribeiro, S.J.L.; André, P.S.; Carlos, L.D.; et al. Sustainable luminescent solar concentrators based on organic–inorganic hybrids modified with chlorophyll. *J. Mater. Chem., A* **2018**, *6*, 8712–8723. [CrossRef]

15. Goetzberger, A.; Greubel, W. Solar-Energy Conversion with Fluorescent Collectors. *Appl. Phys.* **1977**, *14*, 123–139. [CrossRef]

16. Levitt, J.A.; Weber, W.H. Materials for luminescent greenhouse solar collectors. *Appl. Opt.* **1977**, *16*, 2684–2689. [CrossRef] [PubMed]

17. Moraitis, P.; Schropp, R.E.I.; van Sark, W.G.J.H.M. Nanoparticles for Luminescent Solar Concentrators—A review. *Opt. Mater. (Amst).* **2018**, *84*, 636–645. [CrossRef]

18. Brennan, L.J.; Purcell-Milton, F.; McKenna, B.; Watson, T.M.; Gun'ko, Y.K.; Evans, R.C. Large area quantum dot luminescent solar concentrators for use with dye-sensitised solar cells. *J. Mater. Chem. A* **2018**, *6*, 2671–2680. [CrossRef]

19. Shcherbatyuk, G.V.; Inman, R.H.H.; Wang, C.; Winston, R.; Ghosh, S. Viability of using near infrared PbS quantum dots as active materials in luminescent solar concentrators. *Appl. Phys. Lett.* **2010**, *96*, 191901. [CrossRef]

20. Inman, R.H.; Shcherbatyuk, G.V.; Medvedko, D.; Gopinathan, A.; Ghosh, S. Cylindrical luminescent solar concentrators with near-infrared quantum dots. *Opt. Express* **2011**, *19*, 24308–24313. [CrossRef]

21. Zhou, Y.; Benetti, D.; Fan, Z.; Zhao, H.; Ma, D.; Govorov, A.O.; Vomiero, A.; Rosei, F. Near infrared, highly efficient luminescent solar concentrators. *Adv. Energy Mater.* **2016**, *6*, 1501913. [CrossRef]

22. Bottrill, M.; Green, M. Some aspects of quantum dot toxicity. *Chem. Commun.* **2011**, *47*, 7039–7050. [CrossRef]

23. Valizadeh, A.; Mikaeili, H.; Samiei, M.; Farkhani, S.M.; Zarghami, N.; Kouhi, M.; Akbarzadeh, A.; Davaran, S. Quantum dots: synthesis, bioapplications, and toxicity. *Nanoscale Res. Lett.* **2012**, *7*, 480. [CrossRef] [PubMed]

24. Zhang, X.; Wang, T.; Qin, X.; Zhang, Z.; Sun, Y.; Liang, H.; Li, H. Large-area flexible, transparent, and highly luminescent films containing lanthanide (III) complex-doped ionic liquids for efficiency enhancement of silicon-based heterojunction solar cell. *Prog. Photovoltaics Res. Appl.* **2017**, *25*, 1015–1021. [CrossRef]

25. Li, H.; Wang, Y.; Wang, T.; Li, Z. *Ionic Liquids and Rare Earth Soft Luminescent Materials*; Springer: Berlin/Heidelberg, Germany, 2016; pp. 157–178.

26. Ohno, H. *Electrochemical Aspects of Ionic Liquids*; Wiley-Interscience: Hoboken, NJ, USA, 2005; ISBN 9780471762515.

27. Hesemann, P.; Viau, L.; Vioux, A. Silica Ionogels and Ionosilicas. In *The Sol-Gel Handbook*; Wiley-VCH Verlag GmbH & Co. KGaA: Weinheim, Germany, 2015; Volume 2, pp. 487–518. ISBN 9783527334865.

28. Fan, Z.; Wang, Y.; Xue, Z.; Zhang, L.; Chen, Y.; Zhang, S. Preparation, characterization and luminescence of transparent thin film of ionogels. *J. Sol-Gel Sci. Technol.* **2014**, *72*, 328–333. [CrossRef]

29. Zhou, F.; Wang, T.; Li, Z.; Wang, Y. Transparent and luminescent ionogels composed of Eu^{3+}-coordinated ionic liquids and poly(methyl methacrylate). *Luminescence* **2015**, *30*, 1303–1307. [CrossRef] [PubMed]

30. Meinardi, F.; Colombo, A.; Velizhanin, K.A.; Simonutti, R.; Lorenzon, M.; Beverina, L.; Viswanatha, R.; Klimov, V.I.; Brovelli, S. Large-area luminescent solar concentrators based on "Stokes-shift-engineered" nanocrystals in a mass-polymerized PMMA matrix. *Nat. Photonics* **2014**, *8*, 392–399. [CrossRef]

31.　Zettl, M.; Mayer, O.; Klampaftis, E.; Richards, B.S. Investigation of Host Polymers for Luminescent Solar Concentrators. *Energy Technol.* **2017**, *5*, 1037–1044. [CrossRef]

32.　Asghar, M.I.; Zhang, J.; Wang, H.; Lund, P.D. Device stability of perovskite solar cells—A review. *Renew. Sustain. Energy Rev.* **2017**, *77*, 131–146. [CrossRef]

33.　Djurisic, A.B.; Liu, F.Z.; Tam, H.W.; Wong, M.K.; Ng, A.; Surya, C.; Chen, W.; He, Z.B. Perovskite solar cells—An overview of critical issues. *Prog. Quantum Electron.* **2017**, *53*, 1–37. [CrossRef]

34.　Loi, M.A.; Hummelen, J.C. Hybrid solar cells - Perovskites under the Sun. *Nat. Mater.* **2013**, *12*, 1087–1089. [CrossRef]

35.　Frias, A.R.; Cardoso, M.A.; Gonçalves, H.; Correia, S.F.H.; Pereira, R.F.P.; Nunes, S.C.; André, P.S.; Carlos, L.D.; de Zea Bermudez, V.; Ferreira, R.A.S. Transparent luminescent down-shifting layers based on Ln^{3+}-based ionosilicas. 2019; Unpublished work.

36.　Swinehart, D.F. The Beer-Lambert Law. *J. Chem. Educ.* **1962**, *39*, 333–335. [CrossRef]

37.　Reisfeld, R.; Shamrakov, D.; Jorgensen, C. Photostable solar concentrators based on fluorescent glass-films. *Sol. Energy Mater. Sol. Cells* **1994**, *33*, 417–427. [CrossRef]

38.　Correia, S.F.H.; Lima, P.P.; André, P.S.; Ferreira, R.A.S.; Carlos, L.D. High-efficiency luminescent solar concentrators for flexible waveguiding photovoltaics. *Sol. Energy Mater. Sol. Cells* **2015**, *138*, 51–57. [CrossRef]

39.　Afifi, H.H.; Sayyah, S.M.; Higazy, H.; El-Kalla, E.H. Study of the emission spectra of poly(methyl methacrylate) films doped with luminescent materials. *Acta Polym.* **1989**, *40*, 572–575. [CrossRef]

40.　Lima, P.P.; Nobre, S.S.; Freire, R.O.; Alves Junior, S.; Ferreira, R.A.S.; Pischel, U.; Malta, O.L.; Carlos, L.D. Energy transfer mechanisms in organic-inorganic hybrids incorporating europium(III): A quantitative assessment by light emission spectroscopy. *J. Phys. Chem. C* **2007**, *111*, 17627–17634. [CrossRef]

41.　Kai, J.A.; Felinto, M.C.F.C.; Nunes, L.A.O.; Malta, O.L.; Brito, H.F. Intermolecular energy transfer and photostability of luminescence-tuneable multicolour PMMA films doped with lanthanide-beta-diketonate complexes. *J. Mater. Chem.* **2011**, *21*, 3796–3802. [CrossRef]

42.　Fernandes, M.; de Zea Bermudez, V.; Ferreira, R.A.S.; Carlos, L.D.; Charas, A.; Morgado, J.; Silva, M.M.; Smith, M.J. Highly Photostable Luminescent Poly (E-caprolactone) siloxane Biohybrids Doped with Europium Complexes. *Chem. Mater.* **2007**, *19*, 3892–3901. [CrossRef]

43.　Garcia-Torres, J.; Bosch-Jimenez, P.; Torralba-Calleja, E.; Kennedy, M.; Ahmed, H.; Doran, J.; Gutierrez-Tauste, D.; Bautista, L.; Della Pirriera, M. Modulating the photoluminescence of europium-based emitting polymers: Influence of the matrix on the photophysical properties. *J. Photochem. Photobiol. A Chem.* **2014**, *275*, 103–113. [CrossRef]

44.　Moudam, O.; Rowan, B.C.; Alamiry, M.; Richardson, P.; Richards, B.S.; Jones, A.C.; Robertson, N. Europium complexes with high total photoluminescence quantum yields in solution and in PMMA. *Chem. Commun.* **2009**, *43*, 6649–6651. [CrossRef]

45.　Lunstroot, K.; Driesen, K.; Nockemann, P.; Viau, L.; Mutin, P.H.; Vioux, A.; Binnemans, K. Ionic liquid as plasticizer for europium(III)-doped luminescent poly(methyl methacrylate) films. *Phys. Chem. Chem. Phys.* **2010**, *12*, 1879–1885. [CrossRef]

46.　Rondão, R.; Frias, A.R.; Correia, S.F.H.; Fu, L.; de Zea Bermudez, V.; André, P.S.; Ferreira, R.A.S.; Carlos, L.D. High-performance near-infrared luminescent solar concentrators. *ACS Appl. Mater. Interfaces* **2017**, *9*, 12540–12546. [CrossRef]

47.　Latva, M.; Takalo, H.; Mukkala, V.-M.; Matachescu, C.; Rodríguez-Ubis, J.C.; Kankare, J. Correlation between the lowest triplet state energy level of the ligand and lanthanide(III) luminescence quantum yield. *J. Lumin.* **1997**, *75*, 149–169. [CrossRef]

48.　Shavaleev, N.M.; Scopelliti, R.; Gumy, F.; Bünzli, J.-C.G. Near-Infrared Luminescence of Nine-Coordinate Neodymium Complexes with Benzimidazole-Substituted 8-Hydroxyquinolines. *Inorg. Chem.* **2008**, *47*, 9055–9068. [CrossRef] [PubMed]

49.　Biju, S.; Eom, Y.K.; Bünzli, J.-C.G.; Kim, H.K. A new tetrakis β-diketone ligand for NIR emitting LnIII ions: luminescent doped PMMA films and flexible resins for advanced photonic applications. *J. Mater. Chem. C* **2013**, *1*, 6935. [CrossRef]

50.　Biju, S.; Gopakumar, N.; Bünzli, J.-C.G.; Scopelliti, R.; Kim, H.K.; Reddy, M.L.P. Brilliant Photoluminescence and Triboluminescence from Ternary Complexes of Dy [III] and Tb [III] with 3-Phenyl-4-propanoyl-5-isoxazolonate and a Bidentate Phosphine Oxide Coligand. *Inorg. Chem.* **2013**, *52*, 8750–8758. [CrossRef] [PubMed]

51. Malina, I.; Juhnevics, N.; Kampars, V. Study of thermal and optical properties of dibenzoylmethane Eu(III) organic complexes. *Proc. Est. Acad. Sci.* **2017**, *4017*, 493–500. [CrossRef]

52. Ugale, A.; Kalyani, N.T.; Dhoble, S.J. Reddish orange to blue tunable emission from rare earth β-diketonate Eu(TTA)₃dpphen complex for solid state lighting applications. *Mater. Sci. Energy Technol.* **2019**, *2*, 57–66. [CrossRef]

53. Heim, R.; Tsien, R.Y. Engineering green fluorescent protein for improved brightness, longer wavelengths and fluorescence resonance energy transfer. *Curr. Biol.* **1996**, *6*, 178–182. [CrossRef]

54. Butkevich, A.N.; Belov, V.N.; Kolmakov, K.; Sokolov, V.V.; Shojaei, H.; Sidenstein, S.C.; Kamin, D.; Matthias, J.; Vlijm, R.; Engelhardt, J.; et al. Hydroxylated Fluorescent Dyes for Live-Cell Labeling: Synthesis, Spectra and Super-Resolution STED. *Chem. Eur. J.* **2017**, *23*, 12114–12119. [CrossRef]

55. Meinardi, F.; Ehrenberg, S.; Dhamo, L.; Carulli, F.; Mauri, M.; Bruni, F.; Simonutti, R.; Kortshagen, U.; Brovelli, S. Highly efficient luminescent solar concentrators based on earth-abundant indirect-bandgap silicon quantum dots. *Nat. Photonics* **2017**, *11*, 177–185. [CrossRef]

56. Correia, S.F.H.; Lima, P.P.; Pecoraro, E.; Ribeiro, S.J.L.; André, P.S.; Ferreira, R.A.S.; Carlos, L.D. Scale up the collection area of luminescent solar concentrators towards metre-length flexible waveguiding photovoltaics. *Prog. Photovoltaics Res. Appl.* **2016**, *24*, 1178–1193. [CrossRef]

57. Freitas, V.T.; Fu, L.S.; Cojocariu, A.M.; Cattoen, X.; Bartlett, J.R.; Le Parc, R.; Bantignies, J.L.; Man, M.W.C.; Andre, P.S.; Ferreira, R.A.S.; et al. Eu³⁺-based bridged silsesquioxanes for transparent luminescent solar concentrators. *ACS Appl. Mater. Interfaces* **2015**, *7*, 8770–8778. [CrossRef] [PubMed]